Compressive Sensing Ensemble Average Propagator Estimation via L1 Spherical Polar Fourier Imaging

Jian Cheng, Sylvain Merlet, Emmanuel Caruyer, Aurobrata Ghosh, Tianzi Jiang, Rachid Deriche

Compressive Sensing Ensemble Average Propagator Estimation via ℓ_1 Spherical Polar Fourier Imaging

Jian Cheng[1,2], Sylvain Merlet[1], Emmanuel Caruyer[1], Aurobrata Ghosh[1], Tianzi Jiang[2], and Rachid Deriche[1]

[1] Athena Project Team, INRIA Sophia Antipolis – Méditerranée, France,
[2] Center for Computational Medicine, LIAMA, Institute of Automation, Chinese Academy of Sciences, China
Jian.Cheng@inria.fr

Abstract. In diffusion MRI (dMRI) domain, many High Angular Resolution Diffusion Imaging (HARDI) methods were proposed to estimate Ensemble Average Propagator (EAP) and Orientation Distribution Function (ODF). They normally need many samples, which limits their applications. Some Compressive Sensing (CS) based methods were proposed to estimate ODF in Q-Ball Imaging (QBI) from limited samples. However EAP estimation is much more difficult than ODF in QBI. Recently Spherical Polar Fourier Imaging (SPFI) was proposed to represent diffusion signal using Spherical Polar Fourier (SPF) basis without specific assumption on diffusion signals and analytically obtain EAP and ODF via the Fourier dual SPF (dSPF) basis from arbitrarily sampled signal. Normally the coefficients of SPF basis are estimated via Least Square with weighted ℓ_2 norm regularization (ℓ_2-SPFI). However, ℓ_2-SPFI needs a truncated basis to avoid overfitting, which brings some estimation errors. By considering the Fourier relationship between EAP and signal and the Fourier basis pair provided in SPFI, we propose a novel EAP estimation method, named ℓ_1-SPFI, to estimate EAP from limited samples using CS technique, and favorably compare it to the classical ℓ_2-SPFI method. ℓ_1-SPFI estimates the coefficients in SPFI using least square with weighted ℓ_1 norm regularization. The weights are designed to enhance the sparsity. ℓ_1-SPFI significantly accelerates the ordinary CS based Fourier reconstruction method. This is performed by using SPF basis pair in CS estimation process which avoids the numerical Fourier transform in each iteration step. By considering high order basis in ℓ_1 optimization, ℓ_1-SPFI improves EAP reconstruction especially for the angular resolution. The proposed ℓ_1-SPFI was validated by synthetic, phantom and real data. The CS EAP and ODF estimations are discussed in detail and we show that recovering the angular information from CS EAP requires much less samples than *exact* CS EAP reconstruction. Various experiments on synthetic, phantom and real data validate the fact that SPF basis can sparsely represent DW-MRI signals and ℓ_1-SPFI largely improves the CS EAP reconstruction especially the angular resolution.

1 Introduction

Diffusion MRI (dMRI) is to recover the information of biological tissues by modeling water diffusion. Diffusion process is fully described by the Ensemble Average Propagator (EAP) $P(\mathbf{R})$, which is the probability of the displacement vector $\mathbf{R}$ in $\mathbf{R}$-space.

Under the narrow pulse assumption, $P(\mathbf{R})$ in (1) is the Fourier Transform of the signal attenuation $E(\mathbf{q})$ [18], where $\mathbf{q} = q\mathbf{u}$ is the wavevector in $\mathbf{q}$-space, $\mathbf{R} = R\mathbf{r}$.

$$P(\mathbf{R}) = \int E(\mathbf{q}) \exp(-2\pi i \mathbf{q} \cdot \mathbf{R}) \mathrm{d}\mathbf{q}, \tag{1}$$

The most widely used EAP estimation method is Diffusion Tensor Imaging (DTI) [2], which estimates EAP from at least 6 Diffusion Weighted Imaging (DWI) samples by assuming a Gaussian distribution. However, Gaussian assumption can not handle complex fiber configuration. Diffusion Spectrum Imaging (DSI) [18] uses numerical Fourier Transform for EAP estimation. which needs a dense 3D sampling. Q-Ball Imaging (QBI) [16, 9] and Diffusion Orientation Transform (DOT) [13] are two well known single shell High Angular Resolution Imaging (HARDI) method. They estimate ODF and EAP from single shell data. However, QBI suffers from intrinsic modeling error in Funk-Radon Transform and DOT assumes mono-exponential decay. Spherical Polar Fourier Imaging (SPFI) [1, 6, 7], a recent multiple shell HARDI method, was proposed to handle multiple shell (or arbitrarily sampled) data. SPFI can analytically estimate ODF and EAP without any specific assumption by representing the signal $E(\mathbf{q})$ using Spherical Polar Fourier (SPF) basis. A classical Least square method was proposed to estimate the coefficients of SPF basis with weighted ℓ_2 norm regularization [1, 6, 7], which is called ℓ_2-SPFI. Compared to DTI which works with less than 30 samples, HARDI methods like QBI, DOT and SPFI often need about more than 60 DWI samples for ODF/EAP estimation, which limits their application.

Compressive sensing (or compressed sensing) (CS) [5, 4] is a novel technique to robustly reconstruct signal from only a small number of samples when the Nyquist condition is not necessarily met. In MRI field, CS has been successfully applied to reconstruct MRI from measurements in K-space, named Sparse MRI [10]. In dMRI field, [12] used Spherical Ridgelets to recover single shell signal $E(\mathbf{q})$ defined only in $\mathbb{S}^2$ from a small number of samples and estimate ODF by Funk-Radon Transform. However, EAP estimation is much more difficult since it needs to recover $E(\mathbf{q})$ in whole 3D space $\mathbb{R}^3$. [11] is the first paper for CS EAP estimation. It directly applied the Sparse MRI in K-space [10] to $\mathbf{q}$-space for EAP estimation. However, it did not consider any sparse representation of EAP and numerical Fourier Transform is needed in each iteration like Sparse MRI [10].

In this paper, by considering the orthonormal basis pair provided in SPFI, we propose a novel CS EAP estimation method, named ℓ_1-SPFI. It uses least square with weighted ℓ_1 regularization method, also named as Least Absolute Selection and Shrinkage Operator (LASSO) [15, 19], to estimate the coefficients of SPF basis. ℓ_1-SPFI accelerates the ordinary CS method by avoiding numerical Fourier transform in each iteration. The proposed ℓ_1-SPFI was compared with ℓ_2-SPFI [1, 6, 7] in synthetic, phantom and real data.

2 ℓ_2-Spherical Polar Fourier Imaging

SPF basis and Fourier dual SPF basis. SPFI is a model-free, fast, regularized, robust method to estimate EAPs without any specific assumption on signals [1, 6, 7]. In SPFI,

$E(\mathbf{q})$ is represented by an orthonormal basis $\{B_{n,l,m}(\mathbf{q})\}$ in (2), named SPF basis, where ζ is a fixed scale parameter, $R_n(q)$ is the Gaussian-Laguerre (GL) function and $Y_l^m(\mathbf{u})$ is the l order m degree Spherical Harmonic (SH). $\{B_{nlm}\}$ is an orthonormal basis in $\mathbb{R}^3$, which means $E(\mathbf{q})$ can be represented within any given tolerant error if we choose N and L big enough. [7] proved that when the coefficients $\{a_{nlm}\}$ of $E(\mathbf{q})$ under SPF basis are known, the EAP $P(\mathbf{R})$ could be analytically obtained in (4) from the same coefficients $\{a_{nlm}\}$, where ${}_1F_1$ is the confluent hypergeometric function of the first kind.

$$E(q\mathbf{u}) = \sum_{n=0}^{N}\sum_{l=0}^{L}\sum_{m=-l}^{l} a_{n,l,m}R_n(q)Y_l^m(\mathbf{u}) \qquad B_{n,l,m}(\mathbf{q}) = R_n(q)Y_l^m(\mathbf{u}) \tag{2}$$

$$R_n(q) = \kappa_n(\zeta)\exp\left(-\frac{q^2}{2\zeta}\right)L_n^{1/2}(\frac{q^2}{\zeta}) \qquad \kappa_n(\zeta) = \left[\frac{2}{\zeta^{3/2}}\frac{n!}{\Gamma(n+3/2)}\right]^{1/2} \tag{3}$$

$$P(R\mathbf{r}) = \sum_{n=0}^{N}\sum_{l=0}^{L}\sum_{m=-l}^{l} a_{nlm}F_{n,l}(R)Y_l^m(\mathbf{r}) \qquad D_{nlm}(\mathbf{R}) = F_{nl}(R)Y_l^m(\mathbf{r}) \tag{4}$$

$$F_{nl}(R) = \frac{\zeta^{0.5l+1.5}\pi^{l+1.5}R^l\kappa_n(\zeta)}{(-1)^{l/2}\Gamma(l+1.5)}\sum_{i=0}^{n}(-1)^i\binom{n+0.5}{n-i}\frac{1}{i!}2^{0.5l+i+1.5}\Gamma(0.5l+i+1.5){}_1F_1(\frac{2i+l+3}{2};l+\frac{3}{2};-2\pi^2R^2\zeta) \tag{5}$$

Because of Parseval's theorem, i.e. $\delta_{nlm}^{n'l'm'} = \langle B_{nlm}(\mathbf{q})B_{n'l'm'}(\mathbf{q})\rangle = \langle D_{nlm}(\mathbf{R})D_{n'l'm'}(\mathbf{R})\rangle$, $\{D_{nlm}(\mathbf{R})\}$ is actually an orthonormal basis in $\mathbf{R}$ space, called Fourier dual Spherical Polar Fourier (dSPF) basis, So SPFI actually provides two orthonormal basis, i.e. SPF $\{B_{nlm}(\mathbf{q})\}$ in $\mathbf{q}$ space for $E(\mathbf{q})$ and dSPF $\{D_{nlm}(\mathbf{R})\}$ in $\mathbf{R}$ space for $P(\mathbf{R})$. The EAP profile and two kinds of ODFs can be analytically obtained from $\{a_{nlm}\}$ [6, 7]. It has been demonstrated in [1, 6, 7] that the DWI signal $E(\mathbf{q})$ we focus in dMRI could be represented with only a few orders of SPF basis. It works well with $L = 4$ or 6 and $N = 1, 2, 3$ in [1, 6, 7] and the nonzero coefficients concentrate in low orders ($L \leq 8$, $N \leq 4$). That means SPF and dSPF are appropriate sparse bases for $E(\mathbf{q})$ and $P(\mathbf{R})$ based on the definition of sparsity [5, 4]. Please note that although the basis $\{B_{nlm}\}$ with order N and L is used in estimation process, most elements in the estimated coefficients $\{a_{nlm}\}$ ($l \leq L$, $n \leq N$) are actually close to zero, which means again SPF and dSPF basis are appropriate sparse bases. Please see the experiments in Section 4.

ℓ_2-SPFI. The central problem in SPFI is to find a robust and fast estimation of $\{a_{nlm}\}$ from limited number of DWI samples. The classic Least Square estimation with weighted ℓ_2 norm (LS-L2), denoted by ℓ_2-SPFI, is normally used [1, 6, 7]. In ℓ_2-SPFI, coefficient vector $A = (a_{000}, ..., a_{NLL})^T$ is analytically obtained from the solution of LS-L2 problem in (6), which is the regularized solution of the linear system $M_BA = E$.

$$A = \arg\min \|M_BA - E\|_2^2 + A^T\Lambda A = (M_B^TM_B + \Lambda)^{-1}M_B^TE \tag{6}$$

where $E = [E(\mathbf{q}_i)]$ is the signal vector, $M_B = [B_{nlm}(q_i)]$ is the basis matrix and $\Lambda = [\Lambda_{nlm}]$ is the diagonal matrix with two parts of regularization weights, $\Lambda_{nlm} = \lambda_n n^2(n+1)^2 + \lambda_l l^2(l+1)^2$, λ_n and λ_l are regularization parameters for spherical and radial parts. This kind of weighting scheme is motivated by Laplacian-Beltrami regularization in QBI [9] and has been proved useful in [1, 6, 7].

Limitations of ℓ_2-SPFI. Although ℓ_2-SPFI is very fast and works well even for the data with low SNR, low anisotropy and non-exponential decay [6, 7], it has two

natural limitations. *First*, it needs a highly truncated basis, e.g. $N = 1$ and $L = 4$, to avoid overfitting because of limited samples with large noise, which brings some estimation errors and reduces the angular resolution. We may need high order basis for more accurate reconstruction. *Second*, ℓ_2 optimization cannot give a sparse solution for a *exact* reconstruction from limited number of samples based on CS theory [5, 4]. Please see the synthetic data experiments in Section 4.

3 CS EAP Estimation via ℓ_1-Spherical Polar Fourier Imaging

CS Theory. CS theory is a very hot topic nowadays and has many applications [5, 10]. It can robustly and accurately recover signals from undersampling measurements. If the sampling rate is higher than Nyquist rate, the signal can be reconstructed *exactly* by interpolating the samples with sinc function. Shannon sampling theory does not need any assumption. However if some priors of the signal are known, we can do better than Shannon reconstruction. CS theory provides some elegant theoretical tools to *exactly* reconstruct signals based on sparse assumption [5, 4]. A signal, denoted by $f \in \mathbb{R}^N$, is said K-sparse if it has only K nonzero elements with $K \ll N$. Normally the elements of signal are nonzero, but we almost always can choose a good basis $\{\Psi_i(t)\}$ in $\mathbb{R}^N$ to represent the signal with only a small number of coefficients. Then the signal f is called sparse in Ψ domain and it can be represented by coefficient vector x, i.e. $f(t) = \sum_i \Psi_i(t)x_i$, The matrix representation is $f = \Psi x$, where Ψ is the $N \times N$ matrix with $\{\Psi_i\}$ as its columns. Denote Φ as the $M \times N$ measurement matrix and y as the observation vector, i.e. $y = \Phi\Psi x + z$, where z is noise, and $\Theta = \Phi\Psi$ is called the sensing matrix. CS is to recover the coefficients x via ℓ_1 optimization problem in (7), where λ is chosen based on the noise level. It has been proved [5, 4] that if the matrix Θ has good Restricted Isometry Property (RIP), the ℓ_1 optimization is equivalent with L0 optimization and the solution x^* in (7) will be *exact*, i.e. x^* is the the sparse vector in L0 optimization.

$$x^* = \arg\min \|\Theta x - y\|_2^2 + \lambda\|x\|_1 \tag{7}$$

CS EAP Estimation via ℓ_1-SPFI. We aim to reconstruct $P(\mathbf{R})$ from limited samples $\{E(\mathbf{q}_i)\}$ of signal, which is analogous to the reconstruction of MRI signal from K-space measurements in sparse MRI [10]. The EAP $P(\mathbf{R})$ could be seen as the above signal f, and $E(\mathbf{q})$ is the observation vector y in formula (7). The measurement matrix is the undersampled Fourier Transform $F_U = UF$, which first performs a Fourier Transform F and then chooses some samples by undersampling operator U. [11] directly applied sparse MRI to EAP reconstruction, while it did not consider any sparse basis. We propose to represent EAP by dSPF basis $\{D_{nlm}(\mathbf{R})\}$ in (4). Then the coefficient vector of the EAP, denoted by A, can be obtained from the optimization in (8), called ℓ_1-SPFI, where $UFD = M_B$ in (6). The second identity is obtained because the Fourier Transform of $D_{nlm}(\mathbf{R})$ is $B_{nlm}(\mathbf{q})$ [7].

$$A^* = \arg\min \|UFDA - y\|_2^2 + \lambda\|A\|_1 = \arg\min \|M_B A - y\|_2^2 + \lambda\|A\|_1 \tag{8}$$

Formula (8) is actually the well known LASSO method [15]. In statistics, LASSO type estimation in (8) has been widely used and demonstrated significant advantages over the

traditional ridge regression in (6). Moreover please note two important improvement in ℓ_1-SPFI over the CS EAP estimation in [11] by considering sparse basis representation. *First*, [11] discretizes the **R**-space and represented EAP with some discrete samples, which needs many samples to represent continuous EAP and introduces some approximation errors. While in ℓ_1-SPFI, $E(\mathbf{q})$, $P(\mathbf{R})$, $\{B_{nlm}(\mathbf{q})\}$ and $\{D_{nlm}(\mathbf{R})\}$ are all continuous functions in estimation, which avoids discretization. *Second*, normally CS based Fourier reconstructions need to do numerical Fourier Transform in each iterator step [10, 11], which is very slow. While Fourier transform is analytically solved in ℓ_1-SPFI thanks to Fourier basis pair provided in SPFI [7], which significantly accelerates the speed of reconstruction algorithm.

ℓ_1-SPFI with Weighted ℓ_1 Norm. In MRI image recover problem, normally Total Variation term is added in (8) as a sparse term to enhance the sparsity of the solution [10]. However, since in our case EAP is not sparse under Finite Difference and is a "Gaussian-like" smooth function, we do not choose Total Variation term. We use weighted LASSO in (9). The standard LASSO [15] in (8) uses the same weight for different dimension of A. However, it has been demonstrated in [1, 6, 7] that the coefficient A of $E(\mathbf{q})$ concentrates more in low order in both spherical part and radial part of SPF basis, Thus we choose the weight Λ as the same in (6). which will enhance the sparsity of the solution in LASSO [19]. The advantages of this setting over the standard LS-L1 setting in (8) is analogous to the advantages of Laplacian-Beltrami regularization over standard Tikhonov regularization in QBI [9]. Thus compared to ℓ_2-SPFI, instead of LS-L2 in (6) and ordinary LASSO in (8), we propose to estimate A from LS-L1 formulation with weighted ℓ_1 norm in (9). In the following, we will denote the ℓ_1-SPFI with weighted ℓ_1 norm in (9) as ℓ_1-SPFI for simplicity.

$$A^* = \arg\min \|M_B A - E\|_2^2 + \|\Lambda A\|_1 \tag{9}$$

FISTA. Many methods were proposed to solve LS-L1 problem. We use the Fast Iterative shrinkage-thresholding algorithm (FISTA) [3] because it has good rate of convergence. Please note that the original FISTA was proposed for LS-L1 problem with the same weight in each dimension [3]. While different weights are used in (9). Actually the shrinkage operator in FISTA can be splitted for each dimension because ℓ_1 norm is separable. So FISTA can be directly used with different weights. And it works with the same shrinkage procedure and the same rate of convergence as the original FISTA, while no extra computation is added. Please see [3] for more details about FISTA.

Challenges in CS EAP Estimation. EAP estimation is much more difficult than ODF estimation, especially for the ODF in QBI [16, 9]. EAP $P(\mathbf{R})$ is *globally* affected by $E(\mathbf{q})$ defined in whole 3D $\mathbf{q}$ space. An *exact* reconstruction needs to recover $E(\mathbf{q})$ in whole space. Although based on the definition $\frac{1}{Z}\int_0^\infty P(R\mathbf{r})dR$ [16, 9], ODF is still fully determined by $E(\mathbf{q})$ in $\mathbb{R}^3$, many single shell HARDI methods like QBI always use assumptions or make approximations to estimate ODF from only single shell data. It means in single shell HARDI methods like QBI, the estimated ODF from shell q_0 is fully determined by $E(q_0\mathbf{u})$ in $\mathbb{S}^2$. An *exact* reconstruction of such ODF only needs to recover $E(q_0\mathbf{u})$ in $\mathbb{S}^2$, which is much easier and can be performed from very a few samples like in [12]. However, the estimated ODF is just an approximation of the true ODF with some intrinsic modeling error. There are two main challenges of recovering

$E(\mathbf{q})$ in $\mathbb{R}^3$. *First*, it needs more samples in different shells. *Second*, in the shell with large q, signal is very small and SNR is relatively too low. However, many works have good results on angular information even though they made unreasonable approximations like QBI. The fact implies that compared to the fully *exact* EAP reconstruction in $\mathbb{R}^3$, it is probably much easier to recover the angular information of EAP.

4 Experiments

Synthetic data. The synthetic data was generated from mixture of tensor model where two tensors have the same eigenvalues and cross with a given angle in $[45^o, 90^o]$. The eigenvalues are chosen from three configurations, $T1 = (1.7, 0.3, 0.3) \times 10^{-3} mm^2/s$, $T2 = (1.3, 0.4, 0.4) \times 10^{-3} mm^2/s$ and $T3 = (1.1, 0.5, 0.5) \times 10^{-3} mm^2/s$. We compare the proposed ℓ_1-SPFI to ℓ_2-SPFI in different test scenarios with or without Rician noise. Three sampling schemes were used. SS1: 4 shells (b=500/1500/3000/5000 s/mm^2) with 40 samples evenly distributed in each shell. SS2: 3 shells (b=500/1500/3000 s/mm^2) with 40 samples evenly distributed in each shell. SS3: 3 shells (b=500/1500/3000 s/mm^2) with 20 samples evenly distributed in each shell.

In the first experiment, we give an example to show the sparsity of signal/EAP under SPF/dSPF basis and demonstrate the limitations of ℓ_2-SPFI. We first generate diffusion signal $E(\mathbf{q})$ in the whole $\mathbf{q}$-space from two tensors with crossing angle of 90^o and eigenvalues in $T1$, then we perform numerical integration to calculate the ground truth coefficients $\{a_{nlm}\}$ which are the inner products between $E(\mathbf{q})$ and $\{B_{nlm}(\mathbf{q})\}$ because of orthogonality. The first 225 coefficients ($L = 8$, $N = 4$) and the EAP glyph at $15\mu m$ are given in Fig. 1(A). The coefficients for $l > 8, n > 4$ were omitted since they are all zero (numerically very close to zero). The first coefficient for B_{000} is very large, about 350. While only several coefficients for $l \leq 8, n \leq 4$ are larger than 5, and many coefficients are zero (numerically very close to zero). It demonstrates the sparsity of the signal under SPF basis, as well as the sparsity of the EAP under dSPF basis, because these coefficients for signal are also the coefficients for EAP under dSPF basis. Therefore it is possible to estimate EAP via CS technique. We generate noise-free samples in SS1 and estimate the coefficients using ℓ_2-SPFI and ℓ_1-SPFI respectively, where $L = 8$ and $N = 4$ and very little regularization $\lambda_n = \lambda_l = 1e-10$ were chosen. The results were shown in Fig. 1(B) and (C). It is clear to see that with 160 samples in SS1, ℓ_1-SPFI and ℓ_2-SPFI both can *exact* reconstruct the EAP. Fig. 1(D) and (E) are the results from 60 samples in SS3, where $L = 8$ and $N = 4$ and the same regularization $\lambda_n = \lambda_l = 1e - 8$ as [7] were used. ℓ_1-SPFI can obtain sparse result similar with ground truth as expected, while ℓ_2-SPFI obtains noisy result, which explains why L2 regularization methods normally needs a highly truncated basis to force high order coefficients zero [9, 1, 7]. The result from L2-SPFI with truncated basis $L = 4, N = 1$ was shown in Fig. 1(F), which is sparse and the directions are correct. But the glyph is smoother due to the absence of high order information.

So in the following scenarios, we focus on the comparison between ℓ_1-SPFI and ℓ_2-SPFI with truncated basis that was used in practice [1, 7]. We estimate EAP profiles at $R_0 = 15\mu m$, detect the maxima of the profiles based on the method in [9], and calculate the mean difference of angle (MDA) of the detected maxima and the normalized mean

Fig. 1. The coefficients of signal/EAP and the EAP glyphs at $15\mu m$ for the ground truth signal/EAP (A) and estimated signal/EAP (B,C,D,E,F). (B) and (C): the results from SS1 without noise via ℓ_2-SPFI and ℓ_1-SPFI respectively (L=8,N=4). (D) and (E): the results from SS3 with SNR=15 via ℓ_2-SPFI and ℓ_1-SPFI respectively (L=8,N=4). (F): the results from SS3 with SNR=15 via ℓ_2-SPFI with truncated basis (L=4,N=1).

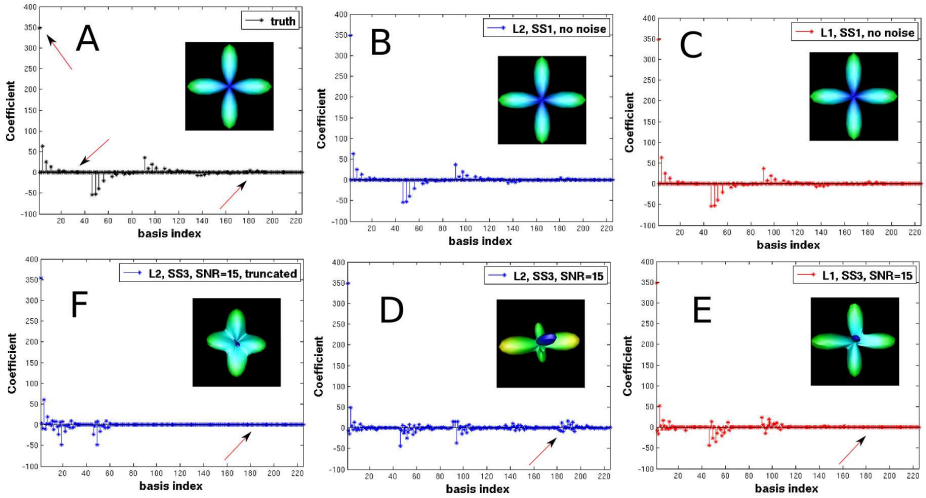

square error (NMSE) between the estimated EAP profile $\widetilde{P}(R_0\mathbf{r})$ and the ground truth $P(R_0\mathbf{r})$. The NMSE is defined as $\frac{\int_{\mathbb{S}^2}|\widetilde{P}(R_0\mathbf{r})-P(R_0\mathbf{r})|^2 d\mathbf{r}}{\int_{\mathbb{S}^2}|P(R_0\mathbf{r})^2 d\mathbf{r}}$.

In the noise free scenario, all three sampling schemes SS1, SS2 and SS3 were used to generate DWI data. In each sampling scheme, all three configurations ($T1$, $T2$ and $T3$) are tested. ℓ_1-SPFI with $L = 8$, $N = 4$ and ℓ_2-SPFI with $L = 4$, $N = 1$ were used to estimate EAPs, where $\lambda_n = \lambda_l = 1e-10$ for both methods because there is no noise. We consider the *exact angular information reconstruction* happens only when 2 maxima are successfully detected *and* the MDA is less than 3^o. And we consider an *exact full reconstruction* happens when *exact angular information reconstruction* happens *and* NMSE is less than 5%. In Fig. 2, A.1, A.2 and A.3 show the NMSE results respectively in SS1, SS2 and SS3 when *exact angular information reconstruction* happens. From the results we have several conclusions. *First*, ℓ_1-SPFI has smaller NMSE and can detect smaller crossing angle than ℓ_2-SPFI in all sampling schemes and tensor configurations. It demonstrates that the high order basis are important for both angular and radial reconstruction for EAPs. *Second*, the results from $T3$ are better than results from $T2$, and the results from $T1$ are worst, which shows ℓ_1-SPFI and ℓ_2-SPFI both work better when $E(\mathbf{q})$ are more isotropic. There is no surprise because the first basis B_{000} and D_{000} which are typical isotropic Gaussian function normally have the largest coefficient. See Fig. 1 for an example. *Third*, an *exact full reconstruction* happens only for $T2$ and $T3$ in SS1 and for $T3$ in SS2 and in SS3. For the more anisotropic EAP from $T1$, we may need more samples for an *exact* reconstruction. *Fourth*, like the experiments in Fig. 1(B) and

Fig. 2. A.1, A.2 and A.3: NMSE in noise free scenario in SS1, SS2 and SS3; B.1 and B.2: successful ratio and MDA in SS1; B.3 and B.4: successful ratio and MDA in SS3;

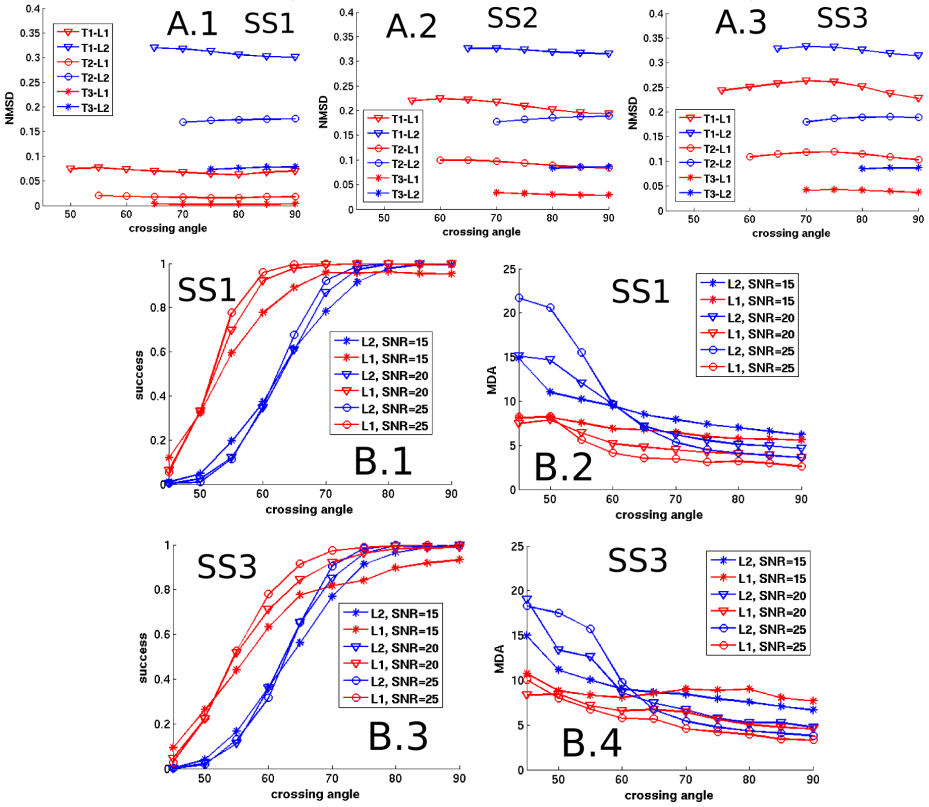

(C), NMSE from SS1 in Fig. 2(A.1) is much small for all tensor configurations and crossing angles, which validates that SPF and dSPF bases are appropriate sparse bases. *Fifth*, sampling in high b values (in SS1) is necessary for an *exact full reconstruction*. Sampling only in low b values ($\leq$ 3000 in SS2 and SS3) largely increases NMSE and slightly reduces MDA. *Sixth*, although only 60 samples were used in SS3, ℓ_1-SPFI still can recover angular information well, which validates the previous discussion that *exact angular information reconstruction* is much easier and needs less samples than an *exact full reconstruction*.

In the noise scenario, SNR is defined as $\frac{1}{\sigma}$, where σ is the deviation of the complex Gaussian noise [9]. The eigenvalue configuration was chosen as $T1$ and we generate data with SNR=15,20,25 in SS1 and SS3 respectively. For every fixed SNR and sampling scheme, Monte Carlo test was performed with 1000 trials to estimate the EAP profiles and detect the maxima. We set $L = 8$, $N = 4$, $\lambda_n = 1e-7$, $\lambda_n = 5e-6$ for ℓ_1-SPFI and $L = 4$, $N = 1$, $\lambda_1 = \lambda_n = 1e-8$ used in [6, 7] for ℓ_2-SPFI. Please note that we may detect more than or less than 2 maxima. The successful ratio to detect 2

maxima was recorded and the MDA was computed as the mean value of differences of angle between detected maxima and the ground truth maxima in the successful tests. Please note the NMSE in the noise scenario normally much large because based on the results in the noise free scenario, *exact full reconstruction* never happens for $T1$ even without noise in SS1, SS2 and SS3. Thus we did not show NMSE in this scenario. See Fig. 2 (B.1-B.4) for results. ℓ_2-SPFI has better results when crossing angle is near 90^o and SNR=15. In other SNR and crossing angles, ℓ_1-SPFI always has higher ratio and smaller MDA. The experiments demonstrate that ℓ_1-SPFI largely improve the reconstruction especially the angular information by considering high order basis in ℓ_1 optimization. ℓ_2-SPFI uses a truncated basis for avoiding overfitting, while ℓ_1-SPFI successfully uses weighted LASSO to avoid overfitting. It should be clarified that although the radial information of EAP may be hard to estimate as we showed, the EAP profile with the angular information was known to have better angular resolution than the ODF [17].

Phantom data. ℓ_1-SPFI was performed in a public phantom data which was used in Fiber Cup in MICCAI 2009 [14]. The data was also used to validate ℓ_2-SPFI in [7]. It has 3 shells (b=500/1500/2000s/mm^2) and each shell has 64 gradients with 2 repetitions. Thus 192 DWIs are obtained as the mean of 2 repetitions. Then we use ℓ_1-SPFI with $L = 8$, $N = 4$, $\lambda_l = 1e-7$, $\lambda_n = 5e-6$ and ℓ_2-SPFI with $L = 4$, $N = 1$, $\lambda_l = 5e-8$, $\lambda_n = 1e-9$ used in [7] to estimate the EAP at $17\mu m$ and $23\mu m$. The results with two enlarged regions (R1 and R2) were visualized in Fig. 3. At $17\mu m$, ℓ_1-SPFI obtains smooth EAPs and ℓ_2-SPFI is better. Compared to ℓ_2-SPFI at $23\mu m$ and $17\mu m$, ℓ_1-SPFI at $23\mu m$ has better results which are more anisotropic with two directions in crossing area and much cleaner in the area known to has one direction. Normally EAPs are estimated around $15\mu m$ and EAPs at $R_0 > 20\mu m$ are likely noisy [7, 13]. However, please note that the phantom data has very low anisotropy so that we need to perform min-max normalization for visualization. Thus we believe for this data it is reasonable that EAP profile is less anisotropic around $15\mu m$ and a larger radius is needed. Moreover, Fig. 3(A) showed the whole field of view for EAPs at $23\mu m$ where the crossing area is obvious *and* other areas are also very clean. That means ℓ_1-SPFI with $23\mu m$ is more robust to noise and more appropriate for this data. In addition we choose 20 gradients per shell via electrostatic energy minimization [8] and use ℓ_1-SPFI again with the same parameters to estimate EAP from only 60 DWIs. The results in two region R1 and R2 from the subset of samples were shown in Fig. 3. EAPs obtained by ℓ_1-SPFI from 60 DWIs, although more noisy, are similar with the results from total 192 DWIs, which demonstrated that the proposed ℓ_1-SPFI, as a CS based method, can robustly estimate the EAP with small number of samples.

Real data. We test ℓ_1-SPFI in a monkey data with 3 shells (b=500,1500,3000s/mm^2) with TE/TR=120ms/6000ms. Each shell has 30 directions. ℓ_1-SPFI was applied to estimate the EAP with $L = 8$, $N = 4$, $\lambda_l = 5e-7$, $\lambda = 5e-6$. The EAP profiles at $15\mu m$ were shown in Fig. 3(B) with an enlarged view (C). The crossing areas could be found. Please note that in both ℓ_2-SPFI [7] and the proposed ℓ_1-SPFI, the EAP profiles in grey matter and CSF area are almost isotropic, which was shown in Fig. 3(E). So for SPFI, min-max normalization is not needed while it is often used for ODFs in QBI [16].

Fig. 3. A: EAPs in whole FOV at 23μm by ℓ_1-SPFI and two enlarged areas (R1, R2) were shown in the following; B: EAPs in whole FOV at 15μm by ℓ_1-SPFI in real data; C: an enlarged area in D.

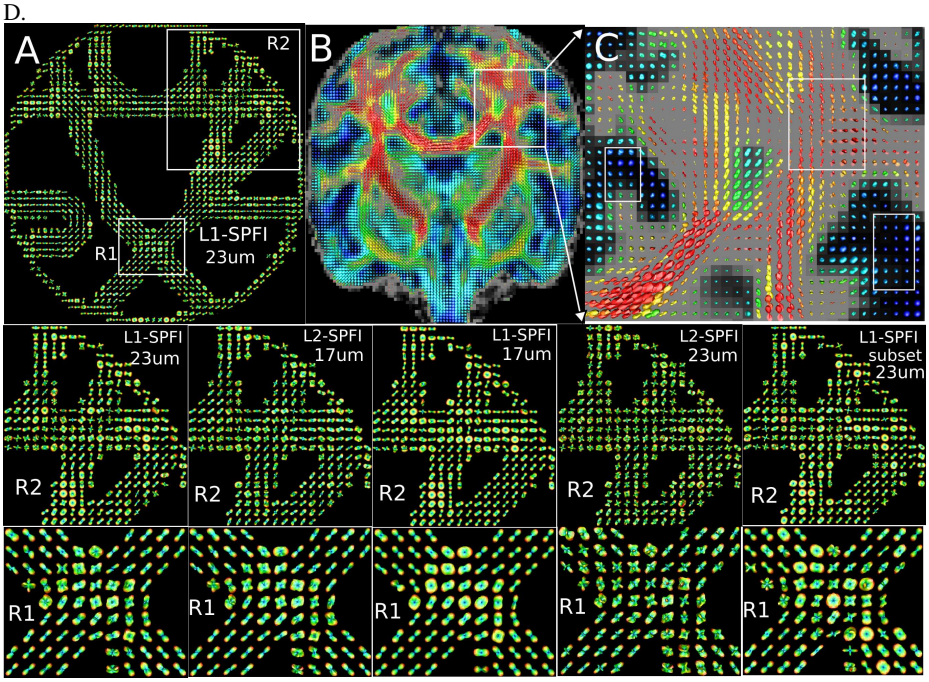

Please note that normalization will make the isotropic area very noisy, which probably brings some troubles for the following fiber tracking method.

5 Conclusion

In this paper, we demonstrate the sparsity of diffusion signal/EAP under SPF/dSPF basis and propose a novel CS based EAP reconstruction method, named as ℓ_1-SPFI, which uses weighted ℓ_1 regularization to estimate the coefficients in SPFI. Compared to ordinary CS Fourier reconstruction methods in [11], it is fast because it avoids numerical Fourier Transform in each iteration by considering the Fourier basis pair provided in SPFI. And it considers continuous EAP in estimation which avoids discretization error. It has been demonstrated that the proposed ℓ_1-SPFI can obtain better results than the ordinary ℓ_2-SPFI when SNR$\geq$ 15. It largely improves the reconstruction especially the angular information by considering high order basis in weighted LASSO. Moreover, we analyzed the differences and challenges in CS EAP estimation compared to CS ODF estimation. We showed that although *exact full reconstruction* of EAP is a challenging problem and needs many samples, ℓ_1-SPFI can recover angular information well from limited samples.

Acknowledgment: This work was partially granted by the French Government Award Program, the Natural Science Foundation of China (30730035,81000634), the National Key Basic Research and Development Program of China (2007CB512305), the French ANR "Neurological and Psychiatric diseases" NucleiPark and the France-Parkinson Association.

References

1. Assemlal, H.E., Tschumperlé, D., Brun, L.: Efficient and robust computation of PDF features from diffusion MR signal. Medical Image Analysis 13, 715–729 (2009)
2. Basser, P.J., Mattiello, J., LeBihan, D.: MR diffusion tensor spectroscropy and imaging. Biophysical Journal 66, 259–267 (1994)
3. Beck, A., Teboulle, M.: A fast iterative shrinkage-thresholding algorithm for linear inverse problems. SIAM Journal on Imaging Sciences 2(1), 183–202 (2009)
4. Candès, E.: Compressive sampling. Proceedings of the International Congress of Mathematicians (2006)
5. Candès, E., Romberg, J., Tao, T.: Robust uncertainty principles: Exact signal reconstruction from highly incomplete frequency information. IEEE Transactions on Information Theory 52(2), 489–509 (2006)
6. Cheng, J., Ghosh, A., Deriche, R., Jiang, T.: Model-free, regularized, fast, and robust analytical orientation distribution function estimation. MICCAI 2010
7. Cheng, J., Ghosh, A., Jiang, T., Deriche, R.: Model-free and analytical EAP reconstruction via spherical polar fourier diffusion mri. MICCAI 2010
8. Cook, P., Symms, M., Boulby, P., Alexander, D.: Optimal acquisition orders of diffusion-weighted MRI measurements. Journal of Magnetic Resonance Imaging 25(5), 1051–1058 (2007)
9. Descoteaux, M., Angelino, E., Fitzgibbons, S., Deriche, R.: Regularized, fast and robust analytical q-ball imaging. Magnetic Resonance in Medicine 58, 497–510 (2007)
10. Lustig, M., Donoho, D., Pauly, J.: Sparse MRI: The application of compressed sensing for rapid MR imaging. Magnetic Resonance in Medicine 58(6), 1182–1195 (2007)
11. Merlet, S., Deriche, R.: Compressed Sensing for Accelerated EAP Recovery in Diffusion MRI. In: Proceedings Computational Diffusion MRI - MICCAI Workshop (2010)
12. Michailovich, O., Rathi, Y.: Fast and accurate reconstruction of HARDI data using compressed sensing. MICCAI 2010
13. Özarslan, E., Shepherd, T.M., Vemuri, B.C., Blackband, S.J., Mareci, T.H.: Resolution of complex tissue microarchitecture using the diffusion orientation transform (DOT). NeuroImage 31, 1086–1103 (2006)
14. Poupon, C., Rieul, B., Kezele, I., Perrin, M., Poupon, F., Mangin, J.: New diffusion phantoms dedicated to the study and validation of high-angular-resolution diffusion imaging (hardi) models. Magnetic Resonance In Medicine 60(6), 1276–1283 (2008)
15. Tibshirani, R.: Regression shrinkage and selection via the lasso. Journal of the Royal Statistical Society. Series B (Methodological) pp. 267–288 (1996)
16. Tuch, D.S.: Q-ball imaging. Magnetic Resonance in Medicine 52, 1358–1372 (2004)
17. Prčkovska, V., Roebroeck, A., Pullens, W., Vilanova, A., ter Haar Romeny, B.: Optimal acquisition schemes in high angular resolution diffusion weighted imaging. MICCAI 2008
18. Wedeen, V.J., Hagmann, P., Tseng, W.Y.I., Reese, T.G., Weisskoff, R.M.: Mapping complex tissue architecture with diffusion spectrum magnetic resonance imaging. Magnetic Resonance In Medicine 54, 1377–1386 (2005)
19. Zou, H.: The adaptive lasso and its oracle properties. Journal of the American Statistical Association 101(476), 1418–1429 (2006)